Volume 236, number 1, 62–70 FEB 06068 August 1988

Refinement of the solution structure of the RNA-DNA hybrid 5′-[r(GCA)d(TGC)]$_2$

Combined use of nuclear magnetic resonance and restrained molecular dynamics

Claudia Scalfi Happ[+], Erwin Happ[+], G. Marius Clore[+°] and Angela M. Gronenborn[+°]

[+] *Max-Planck Institut für Biochemie, D-8033 Martinsried bei München, FRG* and [°] *Laboratory of Chemical Physics, National Institute for Diabetes and Digestive and Kidney Diseases, National Institutes of Health, Bethesda, MD 20892, USA*

Received 4 May 1988

The solution conformation of the self-complementary RNA-DNA hybrid hexamer 5′-[r(GCA)d(TGC)]$_2$ is investigated by NMR spectroscopy and restrained molecular dynamics. The ^{1}H-NMR spectrum is assigned in a sequential manner using two-dimensional homonuclear Hartmann-Hahn and nuclear Overhauser enhancement spectroscopy. From the latter a set of 178 approximate interproton distance restraints are determined and used as the basis of a structure refinement by restrained molecular dynamics. Eight independent calculations are carried out, four from a classical A-type geometry and four from a classical B-type one. Convergence is achieved to very similar A-type structures with an average atomic root mean square difference between them of 1.0 ± 0.2 Å. The converged structures exhibit variations in helical parameters similar to those found previously for the analogue RNA hexamer 5′-r(GCAUGC)$_2$ [(1988) Biochemistry 27, 1735–1743].

RNA-DNA hybrid; Solution conformation; NMR; Interproton distance; Restrained molecular dynamics

1. INTRODUCTION

DNA replication involves the synthesis of intermediates known as Okasaki fragments [1]. These DNA fragments are initiated by a short primer comprising a few ribonucleotides linked covalently to the newly synthesized DNA. A crystallographic study of the decamer hybrid 5′-[r(GCG)d(TATACGC)]$_2$ [2] showed that in the crystal structure both the two DNA-RNA hybrid segments as well as the central DNA-DNA segment adopted an 11-fold A-RNA helical conformation. NMR solution studies on the same oligonucleotide [3] suggested that while the RNA segments were of the A-type, the sugars of the DNA segments retained considerable conformational flexibility.

As part of a continuing study on the conformations of nucleic acids in solution we have investigated the conformation of the RNA-DNA hybrid hexamer 5′-[r(GCA)d(TGC)]$_2$ using a combination of NMR spectroscopy and restrained molecular dynamics. This particular sequence was chosen to enable a direct comparison with the DNA [4] and RNA [5] analogue sequences whose structures we have previously determined by the same methods.

Correspondence address: G.M. Clore or A.M. Gronenborn, Laboratory of Chemical Physics, Building 2, Room 123, National Institute of Diabetes and Digestive and Kidney Diseases, National Institutes of Health, Bethesda, MD 20892, USA

Abbreviations: NMR, nuclear magnetic resonance; NOE, nuclear Overhauser effect; NOESY, two-dimensional NOE spectroscopy; HOHAHA, two-dimensional homonuclear Hartmann-Hahn spectroscopy; rms, root mean square; RD, restrained dynamics

Published by Elsevier Science Publishers B.V. (Biomedical Division)
00145793/88/$3.50

2. EXPERIMENTAL

2.1. *Sample preparation*

The RNA-DNA hybrid hexamer 5′-[r(GCA)d(TGC)]$_2$ was synthesized in solution in a blockwise manner. Ribonucleosides were protected as described previously [6] while the standard benzoyl and isobutyryl protection was used for the deoxyribonucleosides. Further, the terminal deoxycytidine was benzoylated at the 3′-position, and dimethoxytrityl was used for temporary protection of the 5′-OH of thymidine. The two appropriately protected trimers r(GCA) and d(TGC) were prepared by the benzotriazolyl phosphotriester approach [7]. After phosphorylation of the ribo-trimer and detrytilation of the deoxyribo-trimer, the two blocks were condensed in the presence of the 2,4,6-triisopropylbenzenesulfonylchloride and 1-methylimidazole to yield the fully protected hexamer, as described in [8]. Deblocking was carried out in three consecutive steps using oximate, concentrated ammonia and diluted HCl. The crude product was purified by ion-exchange chromatography using a linear gradient of 0.1–0.4 M NaCl as eluant to convert the hexamer into the sodium salt. The hexamer was then desalted initially on a Baker-10 SPE reverse-phase C18 column and finally on a small Sephadex G25 column.

After extensive freeze drying, 125 A_{260} units of the hexamer were dissolved in either 99.995% D_2O or 90% H_2O/10% D_2O containing 25 mM potassium phosphate, 250 mM KCl, 0.025 mM EDTA, pH 6.5, to give a final concentration of ~2.5 mM for the duplex.

The temperature used for all NMR experiments was 25°C; under these conditions the hexamer was entirely double stranded as judged by the observation of three imino proton resonances in 90% H_2O/10% D_2O.

2.2. *NMR spectroscopy*

All NMR spectra were recorded on a Bruker AM500 spectrometer. Two-dimensional NOESY [9] and MLEV17 HOHAHA spectra [10] were recorded in pure-phase absorption mode using the time-proportional incrementation method [11]. Quantification of the NOESY cross-peak intensities was carried out by determining the volume of each cross-peak by two-dimensional integration.

2.3. *Restrained molecular dynamics*

All energy minimization and molecular dynamics calculations were carried out using the program XPLOR [12,13] which is derived from the program CHARMM [14] and has been especially adapted for restrained molecular dynamics. The protocol for the restrained dynamics calculations was essentially as described previously [4,5] with the exception that a square well-potential [15], rather than a skewed biharmonic potential was used for the NOE interproton distance restraints. Restrained molecular dynamics calculations were carried out on a Convex C1-XP computer.

3. RESULTS AND DISCUSSION

3.1. *Sequential resonance assignment and interproton distances*

The assignment of the non-exchangeable protons was accomplished in a sequential manner [16–19] using (a) Hartmann-Hahn spectroscopy to demonstrate direct and relayed through-bond connectivities along the H1′ ↔ H2′/H2′′ ↔ H3′ ↔

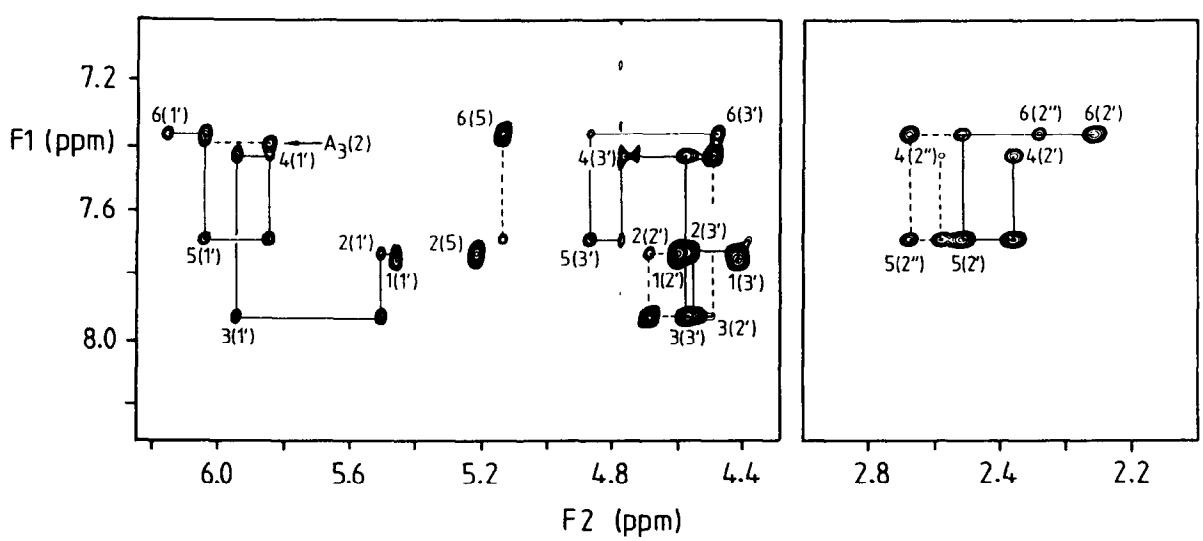

Fig.1. H8/H6 ($F1$ axis)–H5/sugar protons ($F2$ axis) region of the 70 ms NOESY spectrum of the RNA-DNA hybrid hexamer in D_2O. H1′($i-1$) ↔ H8/H6(i) ↔ H1′(i), H2′($i-1$) ↔ H8/H6 (i)↔ H2′(i) and H3′($i-1$) ↔ H8/H6(i) ↔ H3′(i) NOE connectivities are indicated. Intraresidue peaks are labelled according to the resonance on the $F2$ axis. The position along the $F1$ axis of the A_3(H2) resonance is indicated by an arrow.

H4′ ↔ H5′/H5′′ pathway within each sugar unit and (b) NOESY spectroscopy to demonstrate through-space (<5 Å) connectivities along the H1′/H2′/H2′′/H3′($i-1$) ↔ H8/H6(i) ↔ H1′/H2′/H3′(i) pathway. Some examples of NOESY spectra are shown in fig.1.

Interproton distances were determined from the intensities of the cross-peaks in the 70 ms NOESY spectra using the C(H5)–C(H6) and H1′–H2′′ distances (2.45 Å and ~2.3 Å, respectively) and cross-peak intensities as internal references from the equation [20–22]

$$(\langle r_{ij}^{-6}\rangle)^{-1/6} = [a_{H5-H6}(\tau_m)/a_{ij}(\tau_m)]^{-1/6} \cdot r_{H5-H6}$$

(where r_{ij} and $a_{ij}(\tau_m)$ are the distance and NOE cross-peak intensity at a mixing time τ_m, respectively, between protons i and j) on the assumption that the effective correlation times of the $i-j$ and reference interproton vectors are about the same and that the initial rate condition is approximately valid. The validity of the latter assumption for the C(H5)–C(H6) vectors at a mixing time of 70 ms was verified by selective one-dimensional experiments using the NOESY pulse sequence with the first non-selective 90° pulse replaced by a selective 90° Gaussian-shaped pulse [23]. No variation in effective correlation time could be detected from one base to the next. The apparent effective correlation time for the H1′–H2′′ vectors in the deoxyribose section of the hexamer ($r_{H1'-H2''}$ ~ 2.3 Å, independent of sugar pucker conformation), however, was slightly shorter than that of the fixed length C(H5)–C(H6) base vectors. This may well be due to very rapid cross-relaxation between the H2′ and H2′′ sugar protons resulting in small departures from the initial rate approximation for the H1′–H2′′ NOEs. Consequently, all distances involving either the H2′ or H2′′ deoxyribose sugar protons were calculated using the H1′–H2′′ distance and NOE as a reference. (Note that the values of these distances calculated using the C(H5)–C(H6) vector as a reference are only 0.1–0.2 Å longer than those obtained using the H1′–H2′′ vector).

A summary of the calculated interproton distances is given in table 1. Taking into account the errors involved in determining cross-peak intensities by volume integration as well as potential errors arising from possible small variations in effective correlation times and departures from the

Table 1

$(\langle r^{-6}\rangle)^{-1/6}$ mean interproton distances derived from the 70 ms NOESY spectra[a]

(A) Intranucleotide

Proton	r_{ij} (Å)					
	C_1	G_2	A_3	T_4	G_5	C_6
Sugar-sugar						
H1′–H2′	2.6	2.6	2.6	2.8	2.9	2.8
H2′–H2′′				2.3	2.3	2.3
H2′–H3′	2.5		2.5	2.6	2.5	2.5
H2′′–H3′				2.8	2.6	2.7
H1′–H4′	3.6	3.4	3.6	3.3	3.3	3.2
H2′′–H4′				3.1	3.5	3.1
H3′–H4′	2.8			2.6	2.7	2.4
H3′–H5′′					2.9	
H4′–H5′	2.7				2.7	
H4′–H5′′	2.7			2.5	2.7	
Sugar-base						
H1′–H6/H8	3.3	3.9	3.6	3.9	3.6	3.5
H2′–H6/H8	3.3	3.6	4.0	3.0	2.6	3.1
H3′–H6/H8	3.0	2.9	2.8	3.6	3.5	3.0
H5′/H5′′–H6/H8[b]	3.7		3.7	3.9	4.8	3.6

(B) Internucleotide (intrastrand)

Proton of 5′-residue–proton of 3′-residue	r_{ij} (Å)				
	G_1pC_2	C_2pA_3	A_3pU_4	U_4pG_5	G_5pC_6
H1′–H6/H8	3.7	3.5	3.5	3.6	3.5
H2′–H6/H8	2.4	2.4	2.2	2.4	2.8
H2′′–H6/H8				2.9	2.8
H3′–H6/H8	2.9	3.0	3.1	4.1	3.9
H1′–H5					3.7
H2′–H5/CH_3	3.1		3.4		3.5
H2′′–H5/CH_3					3.3
H3′–H5/CH_3	3.3		2.8		3.9
H8/H6–H5/CH_3			3.3		3.9
H2–H1′			3.1		

(C) Internucleotide (interstrand)

Proton	r_{ij} (Å)
A_3H2)–G_{11}(H1′)/A_9H2)–G_5(H1′)	3.7
A_3(H2)–T_{10}(H3)/A_9(H2)–T_4(H3)	2.8

[a] The estimated errors in the distances are as follows: $-0.2/+0.3$ Å for $r_{ij} < 3$ Å, and $-0.3/+0.4$ Å for 3 Å ≤ $r_{ij} \leq 5$ Å. These errors were used to calculate the experimental upper and lower limits of the distance restraints used in the restrained molecular dynamics calculations

[b] In those cases where the H5′ and H5′′ resonances were not stereospecifically assigned, the distances given in the table were set equal to the $\langle r^{-6}\rangle^{-1/6}$ average of the $r_{H5'-H6/H8}$ and $r_{H5''-H6/H8}$ distances

initial rate approximation, we estimate that the errors are -0.2 Å/$+0.3$ Å for $r_{ij} < 3$ Å and -0.3 Å/$+0.4$ Å for 3 Å $\leq r_{ij} < 5$ Å. These errors were subsequently used to determine the upper and lower limits of the experimental interproton distance restraints used in the restrained dynamics calculations.

Information on the C4′–C3′ (δ) bond torsion angle was also deduced from $^3J_{1'2'}$ coupling constants. From the one-dimensional spectrum, these could easily be estimated to be less than 3 Hz for the three ribose units, indicative of a value of $\delta < 100°$ [24].

3.2. *Structure refinement*

In order to obtain the structure of the hexamer in solution we proceeded to carry out restrained molecular dynamics calculations incorporating the experimental interproton distance and δ torsion angle data into the total energy of the system in the form of square well effective potentials (cf. eqns 2 and 3 in [15]). Two initial structures, known as IniA and IniB, were generated from the polar coordinates for classical A- and B-geometries, respectively [25]. The calculations proceeded in three stages: (i) 8 ps of quenched restrained dynamics at 400 K during which time the velocities were rescaled to 400 K every 0.1 ps, the NOE force constant k_{NOE} was increased from 1.0 to 50.0 kcal·mol^{-1}·Å^{-2} by doubling its value every 0.1 ps, and the δ torsion angle restraint force constant for the ribose rings was increased from 1.0 to 40.0 kcal·mol^{-1}·rad^{-2} by multiplying its value by $10^{0.2}$ every 0.1 ps (the values of the restraints force constants reached at the end of this stage were maintained for the rest of the calculation); (ii) 8 ps of quenced restrained dynamics at 300 K in which the velocities were rescaled to 300 K every 0.1 ps; and (iii) 400 cycles of restrained energy minimization of the structure obtained by averaging the coordinate trajectories over the last 6 ps of the second stage. Four calculations were carried out from each initial structure using different random number seeds for the assignments of the initial velocities. The final structures obtained starting from IniA are referred to as ⟨RDA⟩ and those starting from IniB as ⟨RDB⟩; ⟨RDA⟩ and ⟨RDB⟩ are collective referred to as ⟨RD⟩. The coordinates of the 8 final structures were also averaged to yield the average structure $\overline{RD}$ which was subjected to 400 cycles of restrained energy minimization to produce the structure ($\overline{RD}$)m.

The atomic rms differences between the structures are given in table 2, and the rms differences between the calculated and experimental interproton distances, the deviations from ideality for bonds, angles and planes, the NOE and δ restraints energies, and the non-bonding energies are given in table 3. Superpositions of the eight final structures are shown in fig.2.

It is clear from the data in tables 2 and 3 and fig.2 that convergence to essentially the same structures, both globally and locally, has been achieved starting from both initial structures. Further, the atomic rms differences between the final structures are independent of the starting structures. Thus, the difference between the final structures arises from the different random number seeds used to assign the initial velocities. The average atomic rms difference between the final structures is ~1.0 Å and that between the final structures and the mean structure $\overline{RD}$ is ~0.7 Å which is comparable to the atomic rms fluctuations of the atoms about their average positions. The rms difference between the calculated distances and the experimental distance limits (~0.1 Å) is within the experimental errors

Table 2

Atomic rms differences (Å)

Initial and free dynamics structures	
IniA vs IniB	3.22
Rms shifts	
IniA vs ⟨RDA⟩	2.14 ± 0.36
IniB vs ⟨RDB⟩	2.04 ± 0.20
$\overline{RD}$ vs ($\overline{RD}$)m	0.18
Rms distributions	
⟨RDA⟩ vs ⟨RDA⟩	1.12 ± 0.24
⟨RDB⟩ vs ⟨RDB⟩	0.74 ± 0.17
⟨RD⟩ vs ⟨RD⟩	1.00 ± 0.24
⟨RD⟩ vs $\overline{RD}$	0.67 ± 0.15
⟨RD⟩ vs ($\overline{RD}$)m	0.70 ± 0.14

The notation of the structures is as follows: IniA and IniB are the initial structures with regular A and B geometries respectively. ⟨RDA⟩ and ⟨RDB⟩ are the final structures derived from IniA and IniB, respectively; ⟨RD⟩ refers to ⟨RDA⟩ and ⟨RDB⟩ collectively. The atomic standard rms error in the coordinates of the average structure $\overline{RD}$ is given by rmsd/$\sqrt{10}$~0.21 Å, where rmsd is the average atomic rms difference between the eight ⟨RD⟩ structures and the mean structure $\overline{RD}$. ($\overline{RD}$)m is restrained energy minimized average structure obtained by restrained energy minimization of $\overline{RD}$

Table 3

Rms interproton distance deviations, deviations from ideality, and restraints and non-bonding energies for the initial and final structures

Structure	Rms interproton distance deviations (Å)			
	All (194)	Intraresidue (118)	Interresidue (60)	Base-pairing[a] (16)
IniA	0.27 (18)	0.21 (8)	0.39 (10)	0.03 (0)
IniB	0.61 (58)	0.43 (24)	0.92 (34)	0.04 (0)
⟨RD⟩	0.095 ± 0.003 (0)	0.051 ± 0.002 (0)	0.16 ± 0.004 (0)	0.02 ± 0.004 (0)
$\overline{RD}$	0.11 (2)	0.05 (0)	0.19 (2)	0.02 (0)
($\overline{RD}$)m	0.099 (0)	0.05 (0)	0.16 (0)	0.009 (0)

Structure	Deviations from ideality		
	Bonds (*A*) (412)	Angles (°) (738)	Impropers (°)[b] (172)
IniA	0.009	3.14	0.33
IniB	0.008	3.39	0.26
⟨RD⟩	0.009 ± 0	3.49 ± 0.02	0.25 ± 0.022
$\overline{RD}$	0.12	12.84	7.82
($\overline{RD}$)m	0.009	5.07	0.30

Structure	Restraints energy (kcal·mol^{-1})		Non-bonding energy (kcal·mol^{-1})		
	E_{NOE}	E_δ	Van der Waals	Electro-static	H-bond
IniA	432	0	−150	−169	−45
IniB	2112	109	−140	−219	−47
⟨RD⟩	53 ± 5	0 ± 0	−190 ± 2	−218 ± 5	−56 ± 7
RD	74	0	−165	−180	−46
(RD)m	57	0	−192	−205	−56

[a] In addition to the experimental interproton distance restraints, a set of 16 base-pairing restraints corresponding to the base pair hydrogen bonds were added to the NOE restraints energy function. These are as follows: for A·T base pairs $r_{A(N6)-T(O4)}$ = 2.95 Å and $r_{A(N1)-T(H3)}$ = 2.82 Å; for G·C base pairs $r_{G(O6)-C(N4)}$ = 2.91 Å, $r_{G(N1)-C(N3)}$ = 2.95 Å and $r_{G(N2)-C(O2)}$ = 2.86 Å. The values were taken from the X-ray structure analyses of ApU [30] and GpC [31], and the error estimates for these values used in the calculations were ± 0.2 Å

[b] The improper torsion angle restraints are the restraints used to maintain planarity and chirality

[c] The force constant for the NOE restraints k_{NOE} is 50 kcal·mol^{-1}·Å^{-2}

[d] The force constant for the δ torsion angle restraint is 40 kcal·mol^{-1}·rad^{-2}. This is used to restrain the δ torsion angles of the three ribose sugars to <100° on the basis of the small values (<2 Hz) of the $^3J_{1'2'}$ coupling constants

specified and the δ torsion angles lie within the target range.

It should be noted that in the absence of experimental restraints (i.e. using the same dynamics protocol but with the force constants for the NOE and δ torsion angle restraints set to zero) convergence from the two starting structures does not occur. Indeed, the structures diverge (atomic rms difference of 5.4 Å), and the structure starting from IniA remains A-type and that from IniB B-type. Thus, as in the previous cases [4,5,26–28] convergence is entirely due to the incorporation of the experimental restraints into the total energy function of the system in the form of effective

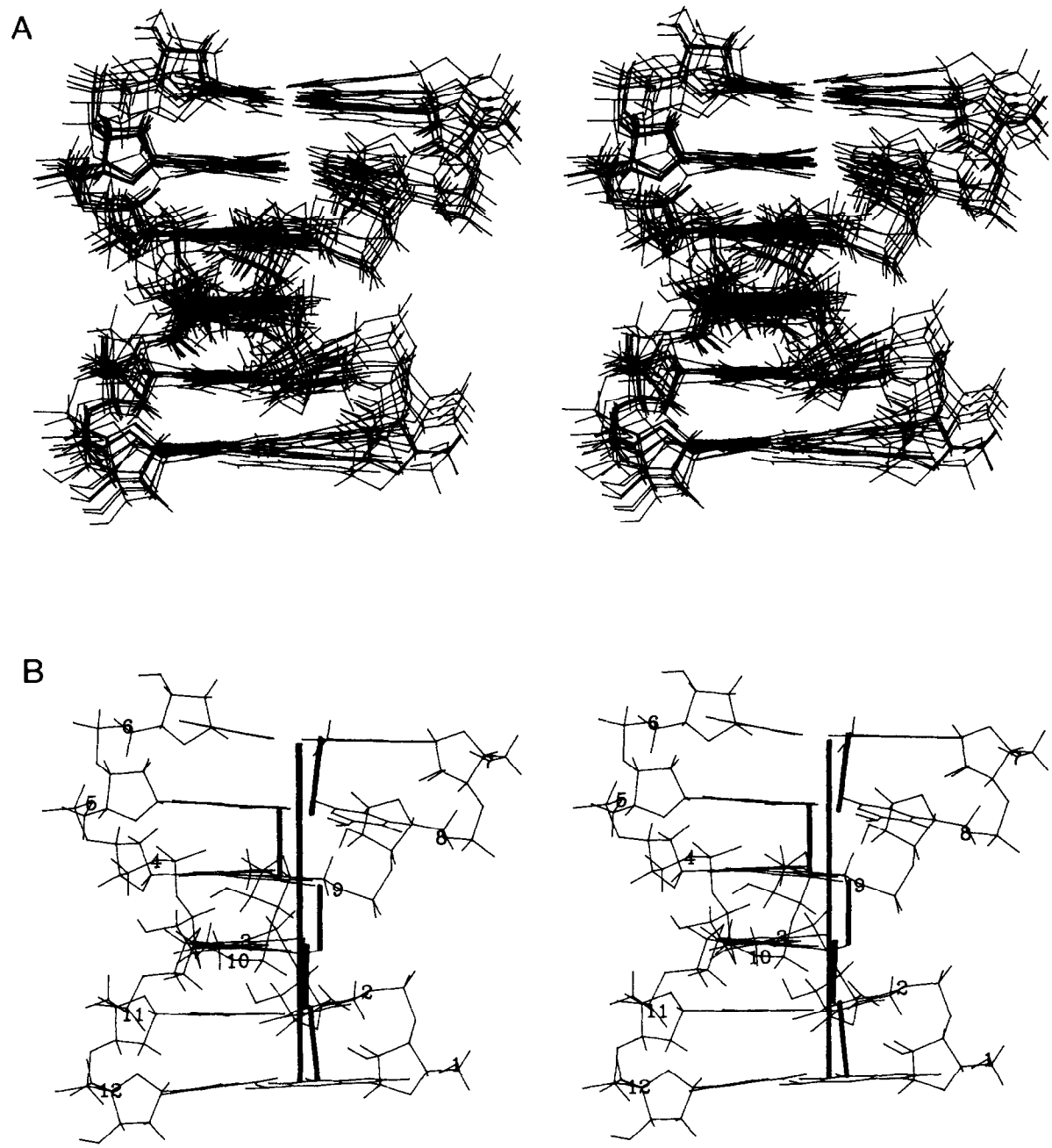

Fig.2. (A) Superposition of the eight converged ⟨RD⟩ structures, and (B) superposition of the global and local helix axes on the restrained energy minimized average structure ($\overline{RD}$)m.

potentials, and the structural features that emerge are not in any way artefacts arising from the empirical energy function. The role of the latter is solely to ensure that the local stereochemistry and non-bonded interactions are approximately correct.

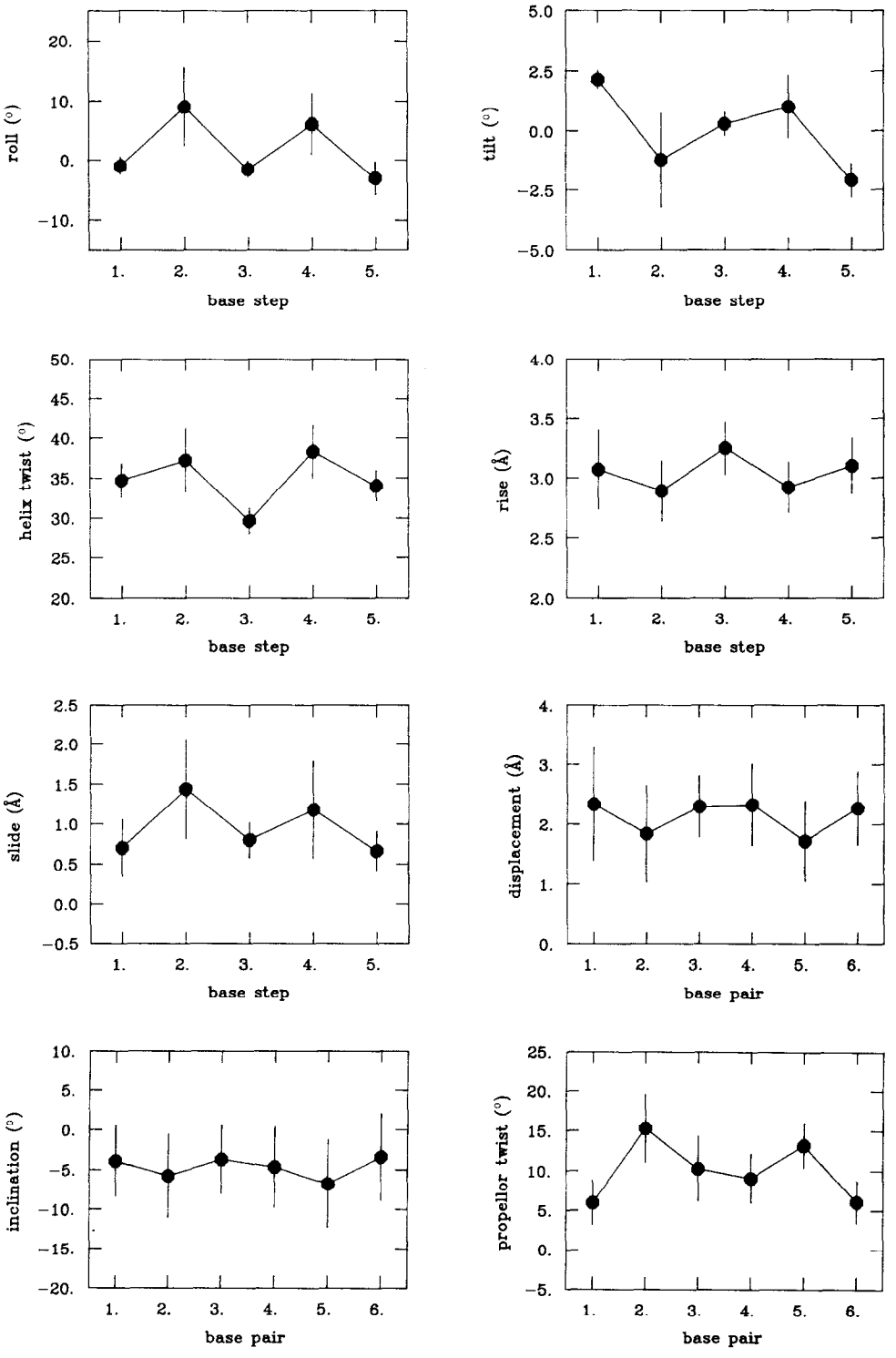

Fig.3. Variations in helical parameters for the eight ⟨RD⟩ converged structures. The solid circles and squares represent the average values and the bars the rms deviations in these values. The exact definitions of the various helical parameters are given in [29].

3.3. *Structural features*

Overall, the structure of the RNA-DNA hybrid hexamer is that of an A-type RNA helix. The atomic rms difference between the restrained energy minimized average structure of the hybrid hexamer and the analogue RNA hexamer [5] is 1.3 Å compared to 1.5 Å versus the analogue DNA hexamer [4]. The variation in backbone torsion angles is small. The glycosidic bond torsion angles tend to be slightly smaller for the DNA nucleotides ($-140 \pm 7°$) than for the RNA ones ($-155 \pm 3°$). The sugar pucker conformation for the ribose rings is consistently 3′-endo, whereas there is some variability in that for the deoxyribose rings. The conformations of the deoxyribose sugars of residues T_4 and G_5 lie in the C1′-exo range, while that of the terminal C_6 residue is 3′-endo. The variation in helical parameters is more significant (fig.3) and is essentially the same as that observed previously for the analogue RNA hexamer [5]. In particular there is an increase in basepair roll, helical twist and base pair slide and a decrease in helical rise at the Pyr_pPur steps. (Note that the analogue DNA hexamer follows exactly the opposite trend for the variation in helical twist.) These structural variations serve to optimize intrastrand stacking of the pyrimidine ring on the six-membered ring of the purine in Pyr_pPur steps, and interstrand stacking of the six-membered rings of the purines in Pur_pPyr steps. Finally, like the RNA hexamer [5], the hybrid hexamer is slightly bent with an angle of ~20° between the local helical axes of base steps 1 and 5 (fig.2). This, however, is much smaller than the value of ~50° found for the analogue DNA hexamer [4].

Thus the results presented in this paper clearly demonstrate that in solution the conformational characteristics of an RNA-DNA hybrid in which the RNA segment lies 5′ to the DNA one, are dominated by the conformational preferences of the RNA component. This is in agreement with the crystallographic findings on another RNA-DNA hybrid [2].

Acknowledgements: This work was supported by the Max-Planck Gesellschaft, grant no. Cl 86/1-1 of the Deutsche Forschungsgemeinschaft, grant no. 321/4003/0318909A from the Bundesministerium für Forschung und Technologie, and the National Institutes of Health (G.M.C. and A.M.G.).

REFERENCES

[1] Ogawa, T. and Okazaki, T. (1980) Annu. Rev. Biochem. 49, 421–457.
[2] Wang, A.H.-J., Fujii, S., Van Boom, J.H., Van der Marel, G.A., Van Boeckel, S.A.A. and Rich, A. (1982) Nature 299, 601–604.
[3] Mellema, J.-R., Haasnoot, C.A.G., Van der Marel, G.A., Wille, G., Van Boeckel, S.A.A., Van Boom, J.H. and Altona, C. (1983) Nucleic Acids Res. 16, 5717–5738.
[4] Nilges, M., Clore, G.M., Gronenborn, A.M., Brünger, A.T., Karplus, M. and Nilsson, L. (1987) Biochemistry 26, 3718–3733.
[5] Scalfi Happ, C., Happ, E., Nilges, M., Gronenborn, A.M. and Clore, G.M. (1988) Biochemistry 27, 1735–1743.
[6] Happ, E., Scalfi Happ, C., Clore, G.M. and Gronenborn, A.M. (1987) Nucleic Acids Res. symposium series no.18, 265–268.
[7] Van Boom, J.H. and Wreesman, C.T.J. (1984) in: Oligonucleotide Synthesis: A Practical Approach (Gait, M.J. ed.) pp.153–183, IRL Press, Oxford.
[8] Efimov, V.A., Reverdatto, S.V. and Chakhmakheheva, O.G. (1982) Nucleic Acids Res. 10, 6675–6694.
[9] Jeener, J., Meier, B.H., Bachmann, P. and Ernst, R.R. (1979) J. Chem. Phys. 71, 4546–4553.
[10] Bax, A. and Davis, D.G. (1985) J. Magn. Reson. 65, 355–360.
[11] Marion, D. and Wüthrich, K. (1983) Biochem. Biophys. Res. Commun. 113, 967–974.
[12] Brünger, A.T., Kuriyan, J. and Karplus, M. (1987) Science 235, 458–460.
[13] Brünger, A.T., Clore, G.M., Gronenborn, A.M. and Karplus, M. (1987) Protein Engin. 1, 399–406.
[14] Brooks, B.R., Bruccoleri, R.E., Olafson, B.D., States, D.J., Swaminathan, S. and Karplus, M. (1983) J. Comput. Chem. 74, 187–217.
[15] Clore, G.M., Nilges, M., Sukumaran, D.K., Brünger, A.T., Karplus, M. and Gronenborn, A.M. (1986) EMBO J. 5, 2729–2735.
[16] Reid, D.G., Salisbury, S.A., Bellard, S., Shakked, Z. and Williams, D.H. (1983) Biochemistry 22, 2019–2025.
[17] Scheek, R.M., Russo, N., Boelens, R., Kaptein, R. and Van Boom, J.H. (1983) J. Am. Chem. Soc. 105, 2914–2916.
[18] Hare, D.R., Wemmer, D.E., Chou, S.H., Drobny, G. and Reid, B.R. (1983) J. Mol. Biol. 171, 319–336.
[19] Clore, G.M. and Gronenborn, A.M. (1983) EMBO J. 2, 2109–2115.
[20] Wagner, G. and Wüthrich, K. (1979) J. Magn. Reson. 33, 675–680.
[21] Dobson, C.M., Olejniczak, E.T., Poulsen, F.M. and Ratcliffe, R.G. (1982) J. Magn. Reson. 48, 87–110.
[22] Clore, G.M. and Gronenborn, A.M. (1985) J. Magn. Reson. 61, 158–164.
[23] Kessler, H., Oschkinat, H., Griesinger, C. and Bermel, W. (1986) J. Magn. Reson. 70, 106–133.
[24] Davies, D.B. (1985) Progr. Nucl. Magn. Reson. Spectroscopy 12, 135–225.
[25] Arnott, S. and Hukins, D.W.L. (1972) Biochem. Biophys. Res. Commun. 47, 1504–1509.

[26] Nilsson, L., Clore, G.M., Gronenborn, A.M., Brünger, A.T. and Karplus, M. (1986) J. Mol. Biol. 188, 455–475.
[27] Nilges, M., Clore, G.M., Gronenborn, A.M., Piel, N. and McLaughlin, L.W. (1987) Biochemistry 26, 3734–3744.
[28] Clore, G.M., Oschkinat, H., McLaughlin, L.W., Benseler, F., Scalfi Happ, C., Happ, E. and Gronenborn, A.M. (1988) Biochemistry 27, 4185–4197.
[29] Dickerson, R.E. (1983) J. Mol. Biol. 166, 419–441.
[30] Seeman, N.C., Rosenberg, J.M., Suddath, F.L., Kim, J.J.P. and Rich, A. (1976) J. Mol. Biol. 104, 109–144.
[31] Rosenberg, J.M., Seeman, N.C., Day, R.O. and Rich, A. (1976) J. Mol. Biol. 104, 145–167.